Increased atmospheric ammonia over the world's major agricultural areas detected from space

J. X. Warner[1], R. R. Dickerson[1], Z. Wei[1], L. L. Strow[2], Y. Wang[3], and Q. Liang[4,5]

[1]Department of Atmospheric and Oceanic Science, University of Maryland College Park, College Park, MD 20742, U.S.A.

[2]Department of Physics and Joint Center for Environmental Technology, University of Maryland Baltimore County, Baltimore, MD 21250, U.S.A.

[3]Department of Earth and Atmospheric Sciences, University of Houston, Houston, TX 77204, U.S.A.

[4]NASA Goddard Space Flight Center, Atmospheric Chemistry and Dynamics, Greenbelt, MD, U.S.A.

[5]Universities Space Research Association, GESTAR, Columbia, MD, USA.

Corresponding author: Juying Warner (juying@atmos.umd.edu)

Key Points:

- First decade-long ammonia records (2002 – 2016) were retrieved from AIRS satellite daily measurements.
- Substantial increases in ammonia concentrations are observed over several of the world's major agricultural regions.
- Causes of ammonia increase include increased fertilizer use, increasing temperatures, and decreased loss to aerosols.

Abstract

This study provides evidence of substantial increases in atmospheric ammonia (NH_3) concentrations (14-year) over several of the worlds major agricultural regions, using recently available retrievals from the Atmospheric Infrared Sounder (AIRS) aboard NASA's Aqua satellite. The main sources of atmospheric NH_3 are farming and animal husbandry involving reactive nitrogen ultimately derived from fertilizer use; rates of emission are also sensitive to climate change. Significant increasing trends are seen over the US (2.61% yr^{-1}), the European Union (EU) (1.83% yr^{-1}), and China (2.27% yr^{-1}). Over the EU, the trend results from decreased scavenging by acid aerosols. Over the US, the increase results from a combination of decreased chemical loss and increased soil temperatures. Over China, decreased chemical loss, increasing temperatures, and increased fertilizer use all play a role. Over South Asia, increased NH_3 emissions are masked by increased SO_2 and NO_x emissions, leading to increased aerosol loading and adverse health effects.

Index terms

Constituent sources and sinks; Troposphere: composition and chemistry; Pollution: urban and regional

Keywords

Ammonia trends; NH_3; ammonium aerosols; SO_2; NO_2; emission

1 Introduction

Atmospheric ammonia (NH_3) is an important component of the global nitrogen cycle [*Galloway et al.*, 2002, 2008; *Sutton et al.*, 2007, 2008; *Erisman et al.*, 2008, 2013; *Fowler et al.*, 2013, 2015]. In the troposphere ammonia reacts rapidly with acids such as sulfuric (H_2SO_4), nitric (HNO_3) to form fine particulate matter ($PM_{2.5}$) [*Malm et al.*, 2004]. These ammonium (NH_4^+) containing aerosols affect Earth's radiative balance, both directly by scattering incoming radiation [*Adams et al.*, 2001; *Martin et al.*, 2004; *Henze et al.*, 2012] and indirectly as cloud condensation nuclei [*Abbatt et al.*, 2006]. $PM_{2.5}$ endangers public health by penetrating the human respiratory systems, depositing in the lungs and alveolar regions [*Pope et al.*, 2002], and causing premature mortality [*Lelieveld et al.*, 2015]. A precursor of these inorganic aerosols, gaseous NH_3 is often the limiting species in their formation [*Wang et al.*, 2013; *Lelieveld et al.*, 2015]. Excess reactive nitrogen reduces biodiversity and causes harmful algal blooms and anoxic conditions. Dry deposition of gaseous ammonia may have substantially greater adverse impacts on ecosystem health than deposition of ammonium in aerosols or precipitation [*Sheppard et al.*, 2011]. In contrast, $PM_{2.5}$ has greater impact on human morbidity and mortality. In this article we quantify recent (~14-year) increases in tropospheric ammonia and suggests likely causes for these trends.

Major sources of atmospheric ammonia involve agricultural activities including animal husbandry, especially concentrated animal feeding operation, and fertilizer use [*Streets et al.*, 2003; *Huang et al.*, 2012; *Hauglustaine et al.*, 2014; *Riddick et al.*, 2016]. Ammonium fertilizers are essential in high-yield crop production, and contribute substantially atmospheric NH_3. Fertilizer usage in China (~31.2 TgN yr^{-1} and ~+2.7% yr^{-1}) and India (~18.8 TgN yr^{-1} and ~+3.6% yr^{-1}) has increase several fold in the last two decades, from Earth Policy Institute (http://www.earth-policy.org/data_highlights/2014/highlights43) and according to the World Bank (http://data.worldbank.org/indicator/AG.CON.FERT.ZS). It is estimated that 50% of the total NH_3 emission in 2000 in China came from fertilizer application and another 38% from other agricultural sources [*Streets et al.*, 2003]. Ammonia emissions increase with increasing nitrogen content and pH of soils and manure storage facilities, and increase exponentially with temperature (emissions roughly double between 300 and 306 K), except below freezing when emissions are near zero [*Riddick et al.*, 2016]. A minimum level of soil moisture is also required for the microbial activities, such as urea hydrolysis, that generate NH_3. Biomass burning, highly episodic in nature, accounts for <10% of the global total, but can be a locally important source [*Dentener and Crutzen*, 1994; *Roelle and Aneja*, 2002; *Galloway et al.*, 2004].

Major sinks of atmospheric ammonia involve dry deposition and wet removal by precipitation, as well as conversion to particulate ammonium by reaction with acids. These acids arise primarily from the oxidation of pollutants SO_2 and NO_x ($NO + NO_2$) generated in the combustion of fossil fuels. Ammonium sulfate is generally removed by precipitation. Condensed ammonium nitrate (NH_4NO_3) exists in equilibrium with NH_3 and gas-phase HNO_3. Lower temperatures favor the aerosol phase.

Measurements of ambient NH_3 are sparse, but satellites provide a means to monitor atmospheric composition globally. Through recent improvements in retrieval algorithms, the Atmospheric Infrared Sounder (AIRS) aboard NASA's Aqua satellite now provides daily global measurement of atmospheric NH_3. Warner et al. [2016] described global NH_3 concentrations using the averaged 13-year satellite data record (2003-2015) from AIRS and provided a global perspective on its emissions, distributions, and spatial variability. They also discussed the

retrieval algorithm, preliminary validation, and qualitative comparisons to measurements from other sensors. In this study, we focus on the NH_3 temporal variability, or trends, from September 2002 to August 2016 and discuss possible mechanisms underlying these trends. These AIRS NH_3 retrievals have greater daily coverages and a longer record than those from the Tropospheric Emission Spectrometer (TES) [Beer et al., 2008]; and are based on higher channel sensitivities, due to the afternoon overpasses, than the Infrared Atmospheric Sounding Interferometer (IASI) [Clarisse et al., 2009]. Van Damme et al. [2015] showed six-year time series of NH_3 total column values over six regions of the world from IASI's early morning (9:30am local time overpass) and evening (9:30pm local time overpass) measurements. Whereas they identified the relatively large emission peaks in the time series as resulting from biomass burning events, their study did not indicate clear increasing or decreasing trends. Schiferl et al. [2016] used a combination of observations (including IASI) and a model to evaluate variability in NH_3 over the US and concluded that variability in meteorology and reduced SO_2 and NO_x emissions drive NH_3 changes observed between 2008 and 2012.

In Section 2, we describe the methods and data used in the analyses, and in Section 3, we present global ammonia trends. In Section 4, we focus on the ammonia trends in the primary regions of interest and discuss the driving mechanisms.

2 Methods and data

2.1 AIRS NH_3 VMRs

Warner et al. [2016] discussed in detail the AIRS NH_3 retrieval method, quality assurance, global NH_3 distributions, and preliminary validation. We applied additional thresholds for the trend computations. We used only NH_3 data with Degree Of Freedom for Signal (DOFS) greater than 0.1, in addition to other retrieval quality assurance flags (e.g., χ^2, retrieval residual, cloud-cleared-radiance quality flags, etc.). All retrieval results were screened by a minimum thermal contrast determined by AIRS L2 products. If the lower layers of the atmosphere and Earth's surface have similar temperatures, (low thermal contrast), they emit similar amounts of thermal radiation [Deeter et al., 2007], and AIRS cannot quantify NH_3 in these layers. While AIRS NH_3 products are outputted at multiple levels from 500 hPa to the surface, here we use NH_3 VMRs at 918 hPa, where the peak sensitivity is, for this study.

For the seasonal cycles, we used a 7-day average for each region and applied an n-point smoothing [Garcia, 2010]. We averaged the seasonal cycles into three periods: from 2002 through 2008, from 2009 through 2013, and from 2014 through 2016, with the mean and the 1-σ standard deviations. Since we only included NH_3 concentrations from frequent sources with elevated NH_3 VMRs, the values shown in all figures maybe higher than the average concentrations in a region.

2.2 Meteorological data sources

As meteorological conditions influence the rate of ammonia emission and deposition, we examine surface skin temperature and total precipitation anomalies using European Centre for Medium-Range Weather Forecasts (ECMWF) era-interim reanalysis (EI) [*Berrisford et al., 2011; Dee et al.,* 2011]. The precipitation anomalies were computed using the 12-hour forecast accumulated in each month for each ECMWF grid (0.75ºx0.75º). Only grids containing AIRS NH_3 retrievals were considered.

For surface skin temperatures anomalies and trends, we selected ECMWF EI daytime data to match the NH_3 daytime product by only using the model outputs between 9am and 3pm local times. Skin temperatures trends were based on daily means and only included the cases with NH_3 retrievals. Additionally, to avoid partial year trends, we use only skin temperatures for the period from March to August when it is sufficiently high to be most relevant to the Northern Hemisphere NH_3 emissions. The linear fits of surface skin temperatures, however, are not statistically significant as indicated by high p-values; they are discussed as references only. We used the published ammonia temperature dependence [*Dentener and Crutzen*, 1994; *Galloway et al.*, 2004; *Riddick et al.*, 2016], with the expression: $E_2 / E_1 = \{\exp [-10380 (1/T_2 - 1/T_1)] - 1\} * 100\%$, where T_1 is assumed to be 300K, T_2 is T_1 plus the observed annual temperature increase, E_1 and E_2 are NH_3 volume mixing ratios corresponding to T_1 and T_2.

2.3 Thermal contrasts

Remote sensing measurement sensitivities depend on surface thermal contrasts of the target areas, and in the case of NH_3, higher thermal contrast generally results in a higher retrieved NH_3 concentrations. Surface thermal contrasts are defined as the differences between surface skin temperatures and surface air temperatures, however, we approximate the ECMWF 2-meter air temperatures as surface air temperatures. While sufficient thermal contrast is needed for good signal-to-noise ratio, the influence of thermal contrast on the retrieved NH_3 concentrations and variability needs to be addressed, especially in trend related studies. When we examine retrievals using separate ranges of thermal contrasts in 2°K degree increments, we found that, although the rates of increase/decrease in NH_3 are different in each thermal contrast range especially during winter season, the tendencies and the magnitudes are similar. Furthermore, the 14-year thermal contrast from ECMWF EI in the regions of our study shows slight decreases (i.e., -0.016ºK yr^{-1}, p=0.002, for the US Midwest, -0.021ºK yr^{-1}, p=0.000, for the EU, -0.011ºK yr^{-1}, p=0.053, for China, and -0.069ºK yr^{-1}, p=0.000, for South Asia). This indicates that the increasing trends of the NH_3 concentrations are not the results of the thermal contrast increasing, since the thermal contrast has decreased. We used thermal contrast daily means in March to August for trend computations and only included regions where there are NH_3 pixels.

2.4 OMI SO_2 and NO_2

We examine ammonia trends jointly with SO_2 and NO_2 changes to determine the scavenging by acid aerosols. We used OMI Level-3 SO_2 planetary boundary layer Volume Column Density (VCD, in DU) spanning October 2005 through August 2016 (http://disc.sci.gsfc.nasa.gov/Aura/data-holdings/OMI/omso2e_v003.shtml). Strong volcanic emissions are removed from the dataset by examining the daily region-wide 99.9-percentile of SO_2 VCDs. If the percentile is found to exceed a threshold value (US 5 DU, Europe 8 DU, China 10 DU, India 8 DU), all data from that day were excluded [*Krotkov, et al.*, 2016]. Note that there are still a few large jumps of SO_2 values associated with volcanic eruptions (e.g., in 2006 and 2008), but volcanoes with a large spatial impact tend to send SO_2 into the upper troposphere where there is little NH_3.

We used OMI cloud-screened tropospheric column NO_2 (molecules/cm^2) datasets similarly to SO_2. As for meteorological variables, SO_2 and NO_2 concentrations were averaged only in the areas where NH_3 retrievals were used. For OMI SO_2, the trends are only significant at

95% confidence level over China. The OMI NO_2 trends are significant at 95% confidence level for the Western US and the EU. The SO_2 concentrations over the US are often below OMI detection limit, and therefore, not used.

3 Observed global ammonia trends

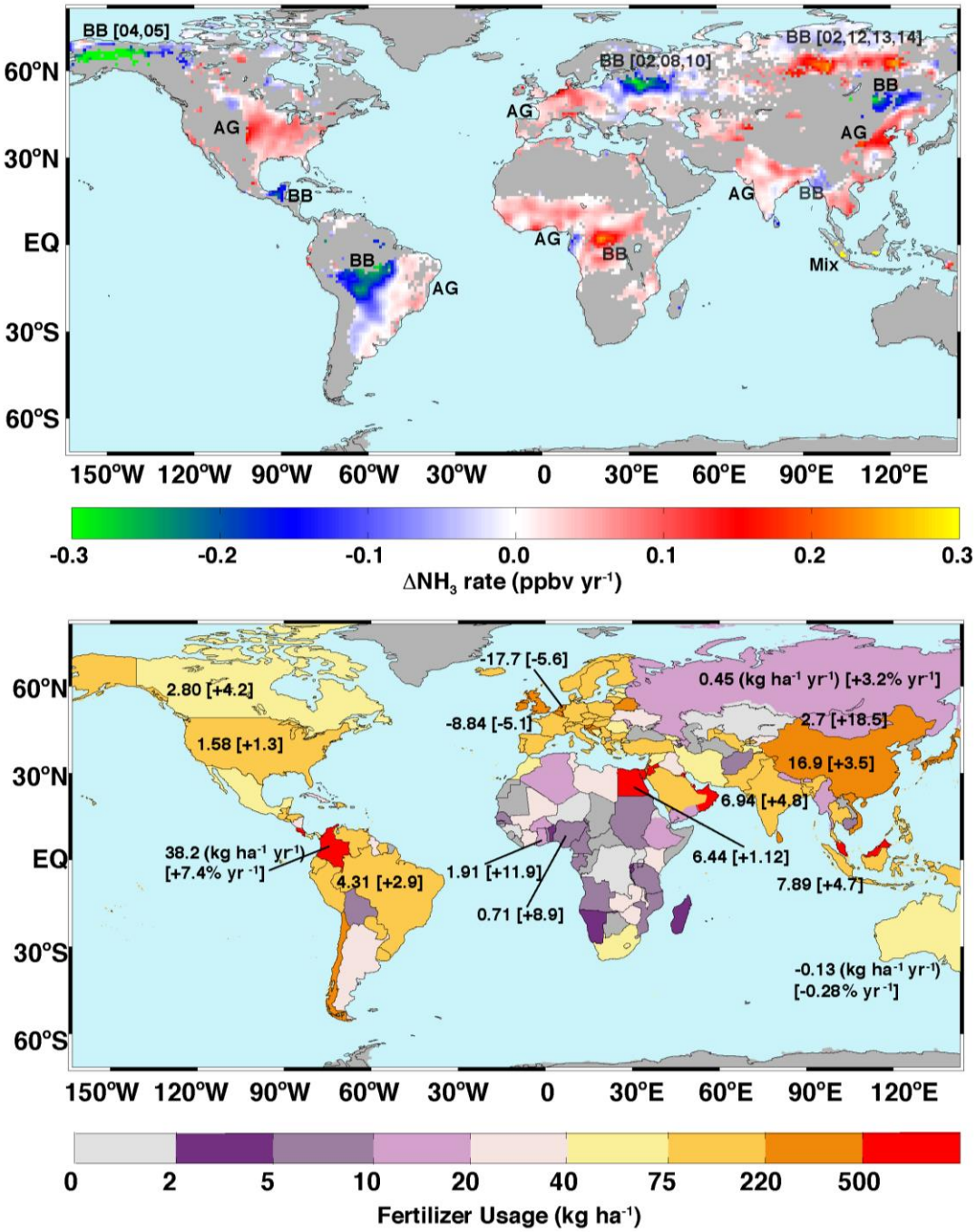

Figure 1. Trend in AIRS NH_3. Top: Temporal trends (+ 0.3 to – 0.3 ppbv yr^{-1}). The locations and the last two digits of the years of biomass burning events (in square brackets) are marked as BB. The main agricultural regions are marked as AG. **Bottom:** national averaged annual N fertilizer usage in 2002 – 2013 in kg ha^{-1} and trends [percentage changes] in kg ha^{-1} yr^{-1} [% yr^{-1}]; see text for details.

Figure 1 top panel depicts a global map of the rate of change of NH_3 volume mixing ratio (VMR) in parts-per-billion by volume (ppbv) per year computed using linear regression of daily mean values in each 1°x1° latitude-longitude grid cell. We used daily mean values in each grid to obtain Fig. 1 top panel. We further smoothed the results using a 2-dimensional penalized least squares method allowing fast smoothing of data in one and higher dimensions by means of the discrete cosine transform [Garcia 2010]. In addition to the general quality assurance described in Methods and Data, we added constraints of only including grids with at least 10% of the pixels greater than 2 ppbv and records longer than 10 years. The years and locations of the biomass burning (BB) events are determined from Moderate Resolution Imaging Spectroradiometer (MODIS) fire products [Giglio et al., 2010] and shown on Fig. 1 top. The main agricultural (AG) regions are determined from Friedl et al. [2010]. The years of the regular fires are not shown. The fertilizer information (i.e., annual usage, trends between 2002 and 2013, and percentage trends) from the World Bank (http://data.worldbank.org/indicator/AG.CON.FERT.ZS) is plotted on Fig. 1 bottom.

AIRS reveals both increases and decreases over disparate parts of the globe. Biomass burning related decreases are seen over Alaska, the central district of Russia and Eastern Europe, Mongolia, Inner Mongolia and NE China, the Yucatan of Mexico, and the Amazon in western Brazil; increases are seen over Siberia and Indonesia. These large fire events are highly episodic, often driven by one or two outlier years (see Fig. 1 top), and are not statistically robust. We focus on regions where such events have minimal influence. Significant NH_3 increases are seen over the American Midwest and southern California (SoCA) (US), east central China, the European Union (EU) countries (e.g., The Netherlands, Germany, Denmark, and Po Valley, Italy), and parts of South Asia (i.e., Bangladesh, India, Pakistan, Cambodia, and Viet Nam), South America (Brazil, Colombia, Ecuador, and parts of Peru), and central Africa (Nigeria, Ghana, Sierra Leone, and Guinea), the Nile Delta of Egypt, and Fergana Valley, Uzbekistan. Regions with increasing trends are generally associated with anthropogenic emissions due to intense agricultural (e.g., related to NH_3 emissions) and changing acid precursor (SO_2 and NO_x) emissions.

Parts of Brazil and parts of Africa have seen substantial increases in ammonia concentrations, but trends in the tropics are complicated by their proximity to major areas of biomass burning, a highly variable source of NH_3. Fertilizer use increase in 2002 – 2013, e.g., 4.3 kg ha^{-1} yr^{-1} (+2.9% yr^{-1}) over Brazil and 0.71 kg ha^{-1} yr^{-1} (+8.9% yr^{-1}) over Nigeria (see Fig. 1 bottom), can largely explain the NH_3 increase over these regions.

4 Regional ammonia trends and their driving mechanisms

Figure 2 left panels show 14-year mean NH_3 VMRs for four regions with intense agricultural activities, the US, China, the EU, and South Asia, where the blue boxes in each panel outline the areas used in the trend computations. The underlying maps were selected using previously defined frequent occurrences of elevated NH_3 concentrations and good measurement sensitivities of AIRS [Warner et al., 2016]. Highest concentrations were observed over densely populated and heavily farmed South Asia followed by Northeast China where a high percentage of land is used for fertilized crops [*Huang et al.*, 2012].

AIRS trend analysis (Fig. 3) shows that NH_3 concentrations have increased over the US by 0.056 ± 0.011 ppbv yr^{-1} (~2. 61% yr^{-1}), over China by 0.076 ± 0. 020 ppbv yr^{-1} (~2. 27% yr^{-1}), and the EU by 0.053 ± 0.021 ppbv yr^{-1} (~1.83% yr^{-1}); error bars represent ± 1 σ standard deviations and the percent increase is based on the mean concentration. The increasing trends in

Fig. 3 are significant at the 95% confidence level for NH_3 over the American Midwest, the EU, and China with p-values at 0.0003, 0.026, and 0.0028, respectively. South Asia shows only a

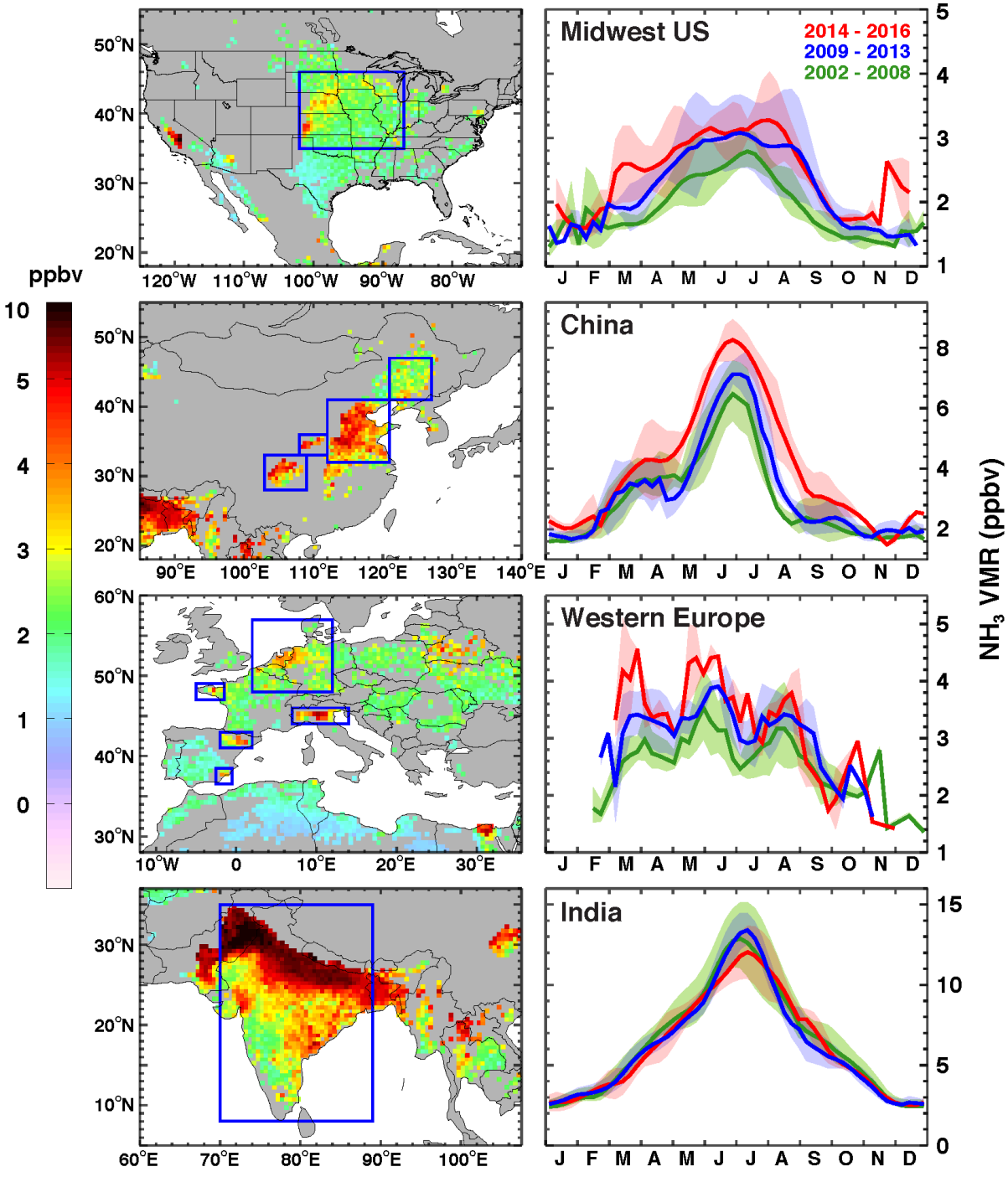

Figure 2. Left: Regions with intense agricultural activities. The averaged 14-year NH_3 VMRs are shown for the American Midwest (top left), China (2nd left), EU (3rd left), and South Asia (bottom left). The blue boxes outline areas used in the trend studies. **Right: The seasonal variability in Midwest U.S. (top right), China (2nd right), EU (3rd right), and South Asia (bottom right).** The 7-day means of NH_3 VMRs at 918 hPa are averaged in 2002 – 2008 (green color), 2009 – 2013 (blue color), and 2014 – 2016 (red color) temporal bands, where broad solid lines represent the averages; and shaded areas are within 1-sigma standard deviations.

slight increase (0.0098 ± 0.019 ppbv yr^{-1}) that is not statistically significant (p-value =0.61). In Fig. 3, the monthly mean AIRS NH_3 VMRs at 918 hPa are plotted from September 2002 to August 2016 with proper quality assurance and screening by frequent occurrences. The trends, however, were linearly fitted using the yearly averaged values.

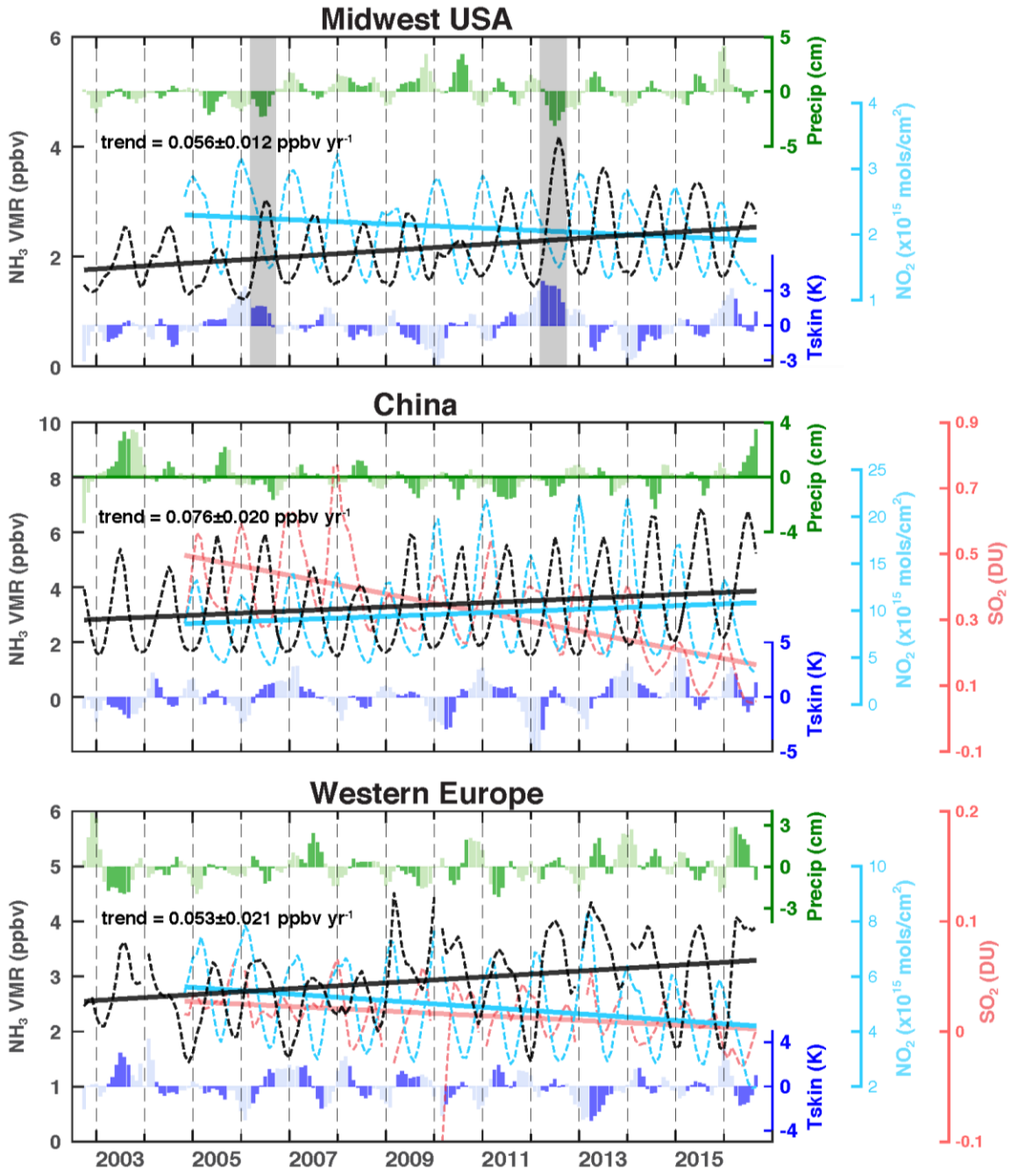

Figure 3. The recent (~14 year) trends of AIRS NH_3 concentrations. The NH_3 concentrations (i.e., VMRs in ppbv) at 918 hPa are shown in black dashed curves, with linear fits in solid lines, for Midwest US (top panel), China (middle panel), and EU (bottom panel) averaged in each region, respectively. The NH_3 increasing trends are correlated with OMI SO_2 decreasing trends (red color curve, shown only for China and EU) and NO_2 trends (cyan

color). Also shown are the surface skin temperature anomaly (K, in blue color bars) and total precipitation anomaly (cm, in green color bars) from the ECMWF era-interim reanalysis.

Over the US, the Midwest shows significant increases in NH_3, but fertilizer use has grown only modestly (~1.3% yr^{-1}) and total food consumption has remained constant within observational uncertainty. Additionally, wet deposition of NH_4^+ does not show any discernable trend [*Lajatha and Jones*, 2013].

What, then is the cause of the definitive growth in the concentration of NH_3? Increases can be attributed to a larger fraction remaining in the gas phase due to decreased removal to the condensed phase. For the period of 2003 to 2014 (latest year for which data are available) the USEPA reports an average NO_2 emissions decreasing at an average of 5.3% yr^{-1} and SO_2 decreasing at 9.0% yr^{-1} (https://www.epa.gov/air-emissions-inventories/air-pollutant-emissions-trends-data). Measurements from the Interagency Monitoring of Protected Visual Environments (IMPROVE) network indicate that US annual mean ambient SO_2 and SO_4^{2-} concentrations have demonstrated consistent decreases [*Hand et al.*, 2012]. Satellite measurements from the Ozone Monitoring Instrument (OMI) [*Krotkov et al.*, 2016] of tropospheric NO_2 indicated a steady decrease (-1.54% yr^{-1}; p-value=0.003) from 2004 to 2016 (Fig. 3, top panel). Emissions of SO_2 and NO_x from the electric power sector in 2012 declined to their lowest level since the passage of the Clean Air Act Amendments of 1990. The sum of emission level of SO_2 and NO_x in 2012 is approximately half of those in 2005 when Clean Air Interstate Rule, a cap-and-trade program intended to reduce SO_2 and NO_x beyond the levels defined by the acid rain program in the eastern half of the US, was announced. The decline in emissions is due primarily to an increasing number of coal-fired units retrofitted with scrubbers, to coal plants switching to lower sulfur coal and low NO_x burners to limit NO_x emissions. Much of the increase in NH_3 over the US, especially after 2011, is thus an unintended consequence of successful measures to control acid deposition.

Year-to-year NH_3 variations over the US are also affected by meteorological conditions. The highest NH_3 concentrations occurred in 2012 when the surface skin temperature anomaly was up to 4 K in the spring and summer months and the total precipitation anomaly was the lowest in the 14-year history (Fig. 3; negative 3 cm; shaded areas). Increased skin temperatures facilitate higher NH_3 emission rates, and decreased precipitation reduces scavenging of NH_3 gas, although a minimal level of soil moisture is necessary for NH_3 release. Hot, dry summers were conducive to high NH_3 concentrations in 2012 and 2006. From September 2002 to August 2016, the average surface skin temperatures in the US Midwest increased by an average of 0.056 K yr^{-1} using March – August data. Using the published ammonia temperature dependence (see section 2.2), we can approximate the contribution from increasing temperatures during this period as 0.65% yr^{-1} or approximately 25% of the total (2.61% yr^{-1}) increase observed. Note that these temperature trends are highly uncertain considering the fitting is not significant (p-value = 0.19). The effects of variability in climate, which strongly influence NH_3 emission, also influence deposition of NH_3 and the partitioning between gas and aerosol phase [*Fowler et al.*, 2015]. Higher air temperatures will reduce the stability of ammonium nitrate aerosols, leading to higher VMRs of NH_3.

The seasonal cycle for the US (Fig. 2 top right panel) shows a broad peak from April to September corresponding to growing season and warmest temperatures; most of the increase is seen in these months. This figure also shows a recent broadening of the maximum, possibly related to warmer temperatures in spring and fall.

Over the EU region, increased NH_3 concentrations appear to be due almost entirely to the decline of SO_2 (-0.0021 ± 0.0007 DU yr^{-1} and -14.12% yr^{-1}) and NO_2 (-0.12 ± 0.0196 $x10^{15}$ molecules/cm^2 yr^{-1} and -2.44% yr^{-1}), according to OMI observations (Fig. 3 bottom panel); aerosol loading over Europe has likewise declined between 1998 and 2010 [*Hsu et al.*, 2012]. A number of regulations on air quality protection existed in EU since 1980, yet a Directive of the European Parliament and of the Council on ambient air quality and cleaner air for Europe was established in 2008 as a basic legal instrument regulating air quality management [Kuklinska et al., 2015]. This new directive obligates the EU members to implement plans to meet the permissible levels of certain substances. Possibly due to this action, as well as the economic crisis, the OMI SO_2 showed a sudden reduction and AIRS NH_3 showed a sudden increase in 2009 and remained at nearly the same level. The relatively small NH_3 increase compared to other major agricultural regions may be partially due to decreases in nitrogenous fertilizer use, e.g., –5.2 kg ha^{-1} yr^{-1} (–0.3% yr^{-1}) from the World Bank 2016 data base and USDA, World Fertilizer Consumption Statistics, and International Fertilizer Industry Association, Paris, 2015 (http://www.fertilizer.org/Statistics). Concentrated animal feeding operations are another major contributor to NH_3 emissions and have increased in the EU countries (e.g., Food And Agriculture Organization Of The United Nations, http://faostat.fao.org) and in the US (http://www.factoryfarmmap.org/-animal:cattle;location:US;year:2012). The surface skin temperature influence on the NH_3 trends in the EU regions was not studied, due to low temperature trends and lack of significance (e.g., -0.0125 K yr^{-1} with p-value = 0.70). The seasonal cycle over the EU (Fig. 2 3rd right panel) is modest, reflecting the weak seasonality in temperature and precipitation.

Over China, the increasing trend of NH_3 (0.076 ppbv yr^{-1}) appears to be related to decreased sulfur emissions, increased fertilizer use, and increasing local temperatures. The OMI SO_2 indicate an irregular but discernable decreasing trend (Fig. 3) while fertilizer application has increased at a rate of 3.5% yr^{-1} over roughly the time period of our AIRS measurements, according to the World Bank (http://data.worldbank.org/indicator/AG.CON.FERT.ZS). Decreases in OMI SO_2 (-0.028 ± 0.0052 DU yr^{-1}, or -8.48% yr^{-1}) (Fig. 3 middle panel) generally track NH_3 increases. An exception to the anti-correlation between SO_2 and NH_3 is the reduction of both species in 2008 driven by aggressive pollution reduction measures associated with the Beijing Olympic Games [*Wang et al.*, 2009]. Chinese pollution control legislations are in 5-year increments, with the 11th five-year plan (FYP) in 2005 – 2010 aiming to reduce SO_2, while the 12th between 2011 and 2015 aiming to reduce SO_2 and NO_x (http://wenku.baidu.com/link?url=LdcQKxIkl-HYhK7uONVne4e5-ikl5Ukvg3iiMVMX37E4LLbIYYfR0s0kdRUbwxydVmZYUcVCFbKyytqxxJPG4kbMQqiUyVahVdc95ZKTiG). The significant SO_2 emission drop in Northeastern China in 2008, and later, are because the 11th FYP mandates the installation of emission control devices for power and steel plants. The NH_3 concentrations increased in 2009 and stayed consistently higher than before 2009 period (see Fig. 2 2nd right panel), correlating well with the SO_2 reduction. The OMI NO_2 shows increases over China through 2014, then a fast decreasing in 2015 and 2016 at the end of the 12th FYP. The NH_3 concentration has reached the highest values in China in 2014, 2015, and 2016 in response to the lowest SO_2 and NO_2 values in our data records. Studies of the response of ammonia emissions to temperature have been conducted primarily in North America and Europe, making extrapolation to Asian soils more uncertain, but if we apply these factors to China, increases in surface skin temperature of 0.0969 K yr^{-1} (p-value = 0.0057) in spring and summer explain an increase of approximately 1.12% yr^{-1} NH_3.

The seasonal cycle over China (Fig. 2 2nd top right panel) shows a sharp peak in June and July corresponding to the warmest temperatures and local precipitation maximum. The monsoons generate a strong seasonal cycle in precipitation not seen over the US or EU. A secondary maximum in spring corresponds to peak fertilizer application. The growing season has broadened over China during the period of study, as was observed for the US.

South Asia (Figs. 2 & 4) shows the highest concentrations and strongest seasonal cycle, but no significant trend over the past 14 years. Heavy fertilizer use and the highest reported number of cattle of any country lead to strong emissions in the warmer months. South Asia has a distinctive monsoon with ~80% of the precipitation falling in between June and September in Delhi. While winters are warm relative to the US, EU, and China, lack of soil moisture inhibits NH_3 production and release. Fertilizer use in South Asia has increased by 6.9 kg ha^{-1} yr^{-1} (+4.8% yr^{-1}) from 2002 to 2013, according to the World Bank. The surface skin temperature influence on the NH_3 trends in South Asia is not studied, due to missing data arising from the uncertainties in summer monsoons, and the small NH_3 trends. Increased emissions are not reflected in the AIRS observations because recent increases in SO_2, 3.25% yr^{-1} (p-value = 0.047), and NO_x, 1.22% yr^{-1} (p-value = 0.0002), from uncontrolled coal combustion and other sources have led to greater conversion of gaseous NH_3 into particulate sulfates and nitrates. Monitoring with sun photometers indicates a substantial increase in aerosol concentrations over recent years [*Hsu et al.*, 2012].

5 Conclusions

The 14-year AIRS satellite record indicates substantial, statistically significant increases in ammonia over several of the world's major agricultural regions, with deleterious effects on vegetation and ecosystem health. Over the US, increases in NH_3 appear to be due to control of SO_2 and NO_x (an unintended consequence of successful acid rain regulations), and to regionally warming temperatures. Over the EU, NH_3 concentrations have increased despite reduced fertilizer use, again due to improved control of sulfur and nitrogen oxide emissions. Over China, a combination of expanded agricultural activities, nascent SO_2 control measures, and increasing temperatures cause the observed increases in ammonia. Over South Asia, increased NH_3 emissions from growing fertilizer use are likely masked by simultaneous increases in SO_2 and NO_x emissions, resulting in increased concentrations of fine aerosols with adverse health effects.

The observed trends deduced here can guide numerical simulation of tropospheric ammonia and inform policy to mitigate disruption of biogeochemical nitrogen cycles and improve air quality. Complete validation of this satellite ammonia product is needed using long-term ground, as well as new airborne measurements as they become available. Ammonia trend monitoring efforts will continue through the lifetime of AIRS sensor, and with current and future operational sensors such as IASI and CrIS (Cross-track Infrared Sounder) preferably using consistent algorithms.

Acknowledgements

This study was funded by NASA's The Science of Terra and Aqua program under grant numbers NNX11AG39G and NNX12AJ05G. We wish to acknowledge the AIRS, OMI, GEOS-Chem, and ECMWF science teams. RRD was a member of AQAST. MERRA data used in this study/project have been provided by GMAO at NASA Goddard Space Flight Center through the

NASA GES DISC online archive. Computations were performed on the NASA Center for Climate Simulation (NCCS) super computing system.

The observational data that support the findings of this study are available on the website via the corresponding author (J.X.W.) (http://atmos.umd.edu/~juying/GRL_2017_AIRS_NH3).

References

Abbatt, J. P. D., S. Benz, D.J. Cziczo, Z. Kanji, U. Lohmann, O. Mohler (2006), Solid Ammonium Sulphate Aerosols as Ice Nuclei: A Pathway for Cirrus Cloud Formation, *Science, 313,* 1770 doi:10.1126/science1129726.

Adams, P. J., J. H. Seinfeld, D. Koch, L. Mickley, and D. Jacob (2001), General circulation model assessment of direct radiative forcing by the sulfate–nitrate–ammonium–water inorganic aerosol system, *J. Geophys. Res.-Atmos., 106*, 1097–1111, doi:10.1029/2000JD900512.

Beer, R., M. W. Shephard, S. S. Kulawik, S. A. Clough, A. Eldering, K. W. Bowman, S. P. Sander, B. M. Fisher, V. H. Payne, M. Luo, G. B. Osterman, and J. R. Worden (2008), First satellite observations of lower tropospheric ammonia and methanol, *Geophys. Res. Lett., 35*, L09801, doi:10.1029/2008GL033642.

Berrisford, P., D. Dee, P. Poli, R. Brugge, K. Fielding, M. Fuentes, P. Kallberg, S. Kobayashi, S. Uppala, and A. Simmons (2011), The ERA-Interim Archive Version 2.0, *ERA Report Series 1, ECMWF,* Shinfield Park. Reading, UK 13177.

Clarisse, L., C. Clerbaux, F. Dentener, D. Hurtmans, and P.-F. Coheur (2009), Global ammonia distribution derived from infrared satellite observations, *Nature Geosci., 2(7),* 479–483, doi:10.1038/ngeo551.

Dee, D. P., S. M. Uppala, A. J. Simmons, P. Berrisford, P. Poli, S. Kobayashi, U. Andreae, M. A. Balmaseda, G. Balsamo, P. Bauer, P. Bechtold, A. C. M. Beljaars, L. van de Berg, J. Bidlot, N. Bormann, C. Delsol, R. Dragani, M. Fuentes, A. J. Geer, L. Haimberger, S. B. Healy, H. Hersbach, E. V. Hólm, L. Isaksen, P. Kållberg, M. Köhler, M. Matricardi, A. P. McNally, B. M. Monge-Sanz, J.-J. Morcrette, B.-K. Park, C. Peubey, P. de Rosnay, C. Tavolato, J.-N. Thépaut, F. Vitart (2011), The ERA-Interim reanalysis: Configuration and performance of the data assimilation system. Quart. *J. R. Meteorol. Soc., 137,* 553-597. DOI: 10.1002/qj.828.

Deeter, M. N., D. P. Edwards, J. C. Gille, and J. R. Drummond (2007), Sensitivity of MOPITT observations to carbon monoxide in the lower troposphere, J. Geophys. Res., 112, D24306, doi:10.1029/2007JD008929.

Dentener, F. J., and P. J. Crutzen (1994), A three-dimensional model of the global ammonia cycle, *J. Atmos. Chem., 19,* 331-369.

Erisman, J. W., M. A. Sutton, J. Galloway, Z. Klimont, and W. Winiwarter (2008), How a century of ammonia synthesis changed the world, *Nature Geosci., 1(10),* 636–639, doi:10.1038/ngeo325.

Erisman, J. W., J. N. Galloway, S. Seitzinger, A. Bleeker, N. B. Dise, R. Petrescu, A. M. Leach, and W. de Vries (2013), Consequences of human modification of the global nitrogen cycle, *Philos. T. R. Soc. B, 368,* 1621, doi:10.1098/rstb.2013.0116.

Fowler D, M. Coyle, U. Skiba, M. A. Sutton, J. N. Cape, S. Reis, L. J. Sheppard, A. Jenkins, B. Grizzetti, J. N. Galloway, P. Vitousek, A. Leach, A. F. Bouwman, K. Butterbach-Bahl, F. Dentener, D. Stevenson, M. Amann, and M. Voss (2013), The global nitrogen cycle in the twenty-first century. *Phil Trans R Soc B 368*, 20130164, doi:10.1098/rstb.2013.0164

Fowler, D., C. E. Steadman, D. Stevenson, M. Coyle, R. M. Rees, U. M. Skiba, M. A. Sutton, J. N. Cape, A. J. Dore, M. Vieno, D. Simpson, S. Zaehle, B. D. Stocker, M. Rinaldi, M. C. Facchini, C. R. Flechard, E. Nemitz, M. Twigg, J. W. Erisman, K. Butterbach-Bahl, and J. N. Galloway (2015), Effects of global change during the 21st century on the nitrogen cycle, *Atmos. Chem. Phys., 15*, 13849–13893, doi:10.5194/acp-15-13849-2015

Friedl, M. A., D. Sulla-Menashe, B. Tan, A. Schneider, N. Ramankutty, A. Sibley, and X. M. Huang (2010), MODIS Collection 5 global land cover: Algorithm refinements and characterization of new datasets, *Remote Sens. Environ.*, *114*(1), 168–182, doi:10.1016/j.rse.2009.08.016.

Galloway, J. N., and E. B. Cowling (2002), Reactive Nitrogen and The World: 200 Years of Change, *Ambio., 31(2),* 64–71, 5 doi:10.1579/0044-7447-31.2.64.

Galloway, J. N., F. J. Dentener, D. G. Capone, E. W. Boyer, R. W. Howarth, S. P. Seitzinger, G. P. Asner, C. C. Cleveland, P. A. Green, E. A. Holland, D. M. Karl, A. F. Michaels, J. H. Porter, A. R. Townsend, C. J. Vöosmarty (2004), Nitrogen cycles: past, present, and future, *Biogeochemistry, 70(2),* 153-226.

Galloway, J. N., A. R. Townsend, J. W. Erisman, M. Bekunda, Z. Cai, J. R. Freney, L. A. Martinelli, S. P. Seitzinger, and M. A. Sutton (2008), Transformation of the nitrogen cycle: Recent trends, questions, and potential solutions, *Science, 320*, 889–892.

Garcia, D. (2010), Robust smoothing of gridded data in one and higher dimensions with missing values. *Comput Stat Data Anal 54*, 1167–1178, doi:10.1016/j.csda.2009.09.020.

Giglio, L., J.T., Randerson, G.R., Van der Werf, P.S., Kasibhatla, G.J., Collatz, D.C., Morton, R.S., DeFries, (2010). Assessing variability and long-term trends in burned area by merging multiple satellite fire products. *Biogeosciences 7*, 1171e1186. http://dx.doi.org/10.5194/bg-7-1171-2010.

Hand, J. L., B. A. Schichtel, W. C. Malm, and M. L. Pitchford (2012), Particulate sulfate ion concentration and SO_2 emission trends in the United States from the early 1990s through 2010, *Atmos. Chem. Phys., 12*, 10353-10365, doi:10.5194/acp-12-10353-2012.

Hauglustaine, D. A., Y. Balkanski, and M. Schulz (2014), A global model simulation of present and future nitrate aerosols and their direct radiative forcing of climate, *Atmos. Chem. Phys., 14*, 11031–11063, doi:10.5194/acp-14-11031-2014.

Henze, D. K., D. T. Shindell, F. Akhtar, R. J. D. Spurr, R. W. Pinder, D. Loughlin, M. Kopacz, K. Sing, and C. Shim (2012), Spatially refined aerosol direct radiative forcing efficiencies, *Environ. Sci. Technol., 46*, 9511–9518, doi:10.1021/es301993s.

Hsu, N. C., R. Gautam, A. M. Sayer, C. Bettenhausen, C. Li, M. J. Jeong, S.-C. Tsay, and B. N. Holben (2012), Global and regional trends of aerosol optical depth over land and ocean using SeaWiFS measurements from 1997 to 2010, *Atmos. Chem. Phys., 12(17)*, 8037-8053.

Huang, X., Y. Song, M. Li, J. Li, Q. Huo, X. Cai, T. Zhu, M. Hu, and H. A. Zhang (2012), High-resolution ammonia emission inventory in China, *Global Biogeochem. Cy., 26*, GB1030, doi:10.1029/2011GB004161.

Krotkov, N. A., C. A. McLinden, C. Li, L. N. Lamsal, E. A. Celarier, S. V. Marchenko, W. H. Swartz, E. J. Bucsela, J. Joiner, B. N. Duncan, K. F. Boersma, J. P. Veefkind, P. F. Levelt, V. E. Fioletov, R. R. Dickerson, H. He, Z. Lu, and D. G. Streets (2016), Aura OMI observations of regional SO_2 and NO_2 pollution changes from 2005 to 2015, *Atmos. Chem. Phys., 16*, 4605-4629, doi:10.5194/acp-16-4605-2016.

Lajtha, K., and J. Jones (2013), Trends in cation, nitrogen, sulfate and hydrogen ion concentrations in precipitation in the United States and Europe from 1978 to 2010: a new look at an old problem, *Biogeochemistry, 116(1-3),* 303-334.

Lelieveld, J., J. S. Evans, M. Fnais, D. Giannadaki, and A. Pozzer (2015), The contribution of outdoor air pollution sources to premature mortality on a global scale. *Nature, 525.7569,* 367-371.

Malm, W. C., B. A. Schichtel, M. L. Pitchford, L. L. Ashbaugh, and R. A. Eldred (2004), Spatial and monthly trends in speciated fine particle concentration in the United States, *J. Geophys. Res. 109*, D03306, doi:10.1029/2003JD003739.

Martin, S. T., Hung, H.-M., Park, R. J., Jacob, D. J., Spurr, R. J. D., Chance, K. V., and Chin, M. (2004), Effects of the physical state of tropospheric ammonium-sulfate-nitrate particles on global aerosol direct radiative forcing, *Atmos. Chem. Phys., 4,* 183–214, doi:10.5194/acp-4-183-2004.

Pope, C. A., Burnett, R. T., Thun, M. J., Calle, E. E., Krewski, D., Ito, K., and Thurston, G. D. (2002), Lung cancer, cardiopulmonary, mortality, and long-term exposure to fine particulate air pollution, *J. Am. Med. Assoc., 287,* 1132–1141.

Riddick, S., Ward, D., Hess, P., Mahowald, N., Massad, R., and Holland, E. (2016), Estimate of changes in agricultural terrestrial nitrogen pathways and ammonia emissions from 1850 to present in the Community Earth System Model, *Biogeosciences, 13(11),* 3397-3426.

Roelle, P. A. and Aneja, V. P. (2002), Environmental Simulation Chambers: Application to Atmospheric Chemical Processes, *Science, 457 pp.* (Springer, 13 January 2006).

Schiferl, L. D., Heald, C. L., Van Damme, M., Clarisse, L., Clerbaux, C., Coheur, P.-F., Nowak, J. B., Neuman, J. A., Herndon, S. C., Roscioli, J. R., and Eilerman, S. J. (2016): Interannual variability of ammonia concentrations over the United States: sources and implications, Atmos. Chem. Phys., 16, 12305-12328, doi:10.5194/acp-16-12305-2016.

Sheppard L. J., Leith, I. D., Mizunuma, T., Cape, J. N., Crossley, A., Leeson, S., Sutton, M. A., Dijk, N. V., and Fowler, D. (2011), Dry deposition of ammonia gas drives species change faster than wet deposition of ammonium ions: evidence from a long-term field manipulation, *Global Change Biology, 17,* 3589–3607, doi:10.1111/j.1365-2486.2011.02478.x.

Streets, D. G., Bond, T. C., Carmichael, G. R., Fernandes, S. D., Fu, Q., He, D., Klimont, Z., Nelson, S. M., Tsai, N. Y., Wang, M. Q., Woo, J. H., and Yarber, K. F. (2003), An inventory of gaseous and primary aerosol emissions in Asia in the year 2000, *J. Geophys. Res.-Atmos., 108(D21),* 8809, doi:10.1029/2002JD003093.

508 Sutton, M. A., Nemitz, E., Erisman, J. W., Beier, C., Bahl, K. B., Cellier, P., de Vries, W.,
509 Cotrufo, F., Skiba, U., Di Marco, C., Jones, S., Laville, P., Soussana, J. F., Loubet, B.,
510 Twigg, M., Famulari, D., Whitehead, J., Gallagher, M. W., Neftel, A., Flechard, C. R.,
511 Herrmann, B., Calanca, P. L., Schjoerring, J. K., Daemmgen, U., Horvath, L., Tang, Y. S.,
512 Emmett, B. A., Tietema, A., Penuelas, J., Kesik, M., Brueggemann, N., Pilegaard, K.,
513 Vesala, T., Campbell, C. L., Olesen, J. E., Dragosits, U., Theobald, M. R., Levy, P., Mobbs,
514 D. C., Milne, R., Viovy, N., Vuichard, N., Smith, J. U., Smith, P., Bergamaschi, P., Fowler,
515 D., and Reis, S. (2007), Challenges in quantifying biosphere-atmosphere exchange of
516 nitrogen species, *Environ. Pollut., 150,* 125–139, doi:10.1016/j.envpol.2007.04.014.

517 Sutton, M., Erisman, J., Dentener, F., and Moller, D. (2008), Ammonia in the environment: From
518 ancient times to the present, *Environ. Pollut., 156,* 583–604,
519 doi:10.1016/j.envpol.2008.03.013.

520 Van Damme, M., Erisman, J. W., Clarisse, L., Dammers, E., Whitburn, S., Clerbaux, C.,
521 Dolman, A. J., and Coheur, P.-F. (2015), Worldwide spatiotemporal atmospheric ammonia
522 (NH3) columns variability revealed by satellite, Geophys. Res. Lett., 42(20), 8660–8668,
523 doi:10.1002/2015GL065496.

524 Wang, Y., Hao, J., McElroy, M. B., Munger, J. W., Ma, H., Chen, D., & Nielsen, C. P. (2009),
525 Ozone air quality during the 2008 Beijing Olympics: effectiveness of emission restrictions,
526 *Atmos. Chem. Phys., 9(14),* 5237-5251.

527 Wang, Y., Zhang, Q. Q., He, K., Zhang, Q., and Chai, L. (2013), Sulfate-nitrate-ammonium
528 aerosols over China: response to 2000–2015 emission changes of sulfur dioxide, nitrogen
529 oxides, and ammonia, *Atmos. Chem. Phys., 13,* 2635-2652, doi:10.5194/acp-13-2635-2013.

530 Warner, J. X., Wei, Z., Strow, L. L., Dickerson, R. R., Nowak, R. (2016), Global Ammonia
531 Sources Seen by AIRS 13-years Measurements, *Atmos. Chem. Phys. 16,* 5467-
532 5479, doi:10.5194/acp-16-5467-2016.